Efficient topology-aware simplification of large triangulated terrains

Yunting Song
University of Maryland
College Park, Maryland, USA
ytsong@umd.edu

Riccardo Fellegara
German Aerospace Center (DLR)
Braunschweig, Germany
riccardo.fellegara@dlr.de

Federico Iuricich
Clemson University
Clemson, South Carolina, USA
fiurici@clemson.edu

Leila De Floriani
University of Maryland
College Park, Maryland, USA
deflo@umd.edu

ABSTRACT

A common first step in the terrain processing pipeline of large Triangulated Irregular Networks (TINs) is simplifying the TIN to make it manageable for further processing. The major problem with TIN simplification algorithms is that they create or remove critical points in an uncontrolled way. Topology-aware operators have been defined to solve this issue by coarsening a TIN without affecting the topology of its underlying terrain, i.e., without modifying critical simplices describing pits, saddles, peaks, and their connectivity. While effective, existing algorithms are sequential in nature and are not scalable enough to perform well with large terrains on multicore systems. Here, we consider the problem of topology-aware simplification of very large meshes. We define a topology-aware simplification algorithm on a compact and distributed data structure for triangle meshes, namely the Terrain trees. Terrain trees reduce both the memory and time requirements of the simplification procedure by adopting a batched processing strategy of the mesh elements. Furthermore, we define a new parallel topology-aware simplification algorithm that takes advantage of the spatial domain decomposition at the basis of Terrain trees. Scalability and efficiency are experimentally demonstrated on real-world TINs originated from topographic and bathymetric LiDAR data. Our experiments show that topology-aware simplification on Terrain trees uses 40% less memory and half the time than the same approach implemented on the most compact and efficient connectivity-based data structure for TINs. Beyond that, our parallel algorithm on the Terrain trees reaches a 12x speedup when using 20 threads.

CCS CONCEPTS

• **Computing methodologies** → **Mesh geometry models**; *Shape analysis*; • **Information systems** → **Data structures**; *Geographic information systems.*

KEYWORDS

terrain simplification, edge contraction, spatial indexes, topological methods, shared memory processing

ACM Reference Format:
Yunting Song, Riccardo Fellegara, Federico Iuricich, and Leila De Floriani. 2021. Efficient topology-aware simplification of large triangulated terrains. In *29th International Conference on Advances in Geographic Information Systems (SIGSPATIAL '21), November 2–5, 2021, Beijing, China.* ACM, New York, NY, USA, 12 pages. https://doi.org/10.1145/3474717.3484261

1 INTRODUCTION

Morse theory is a powerful mathematical framework that allows for segmenting a scalar field according to the regions of influence of its critical points. This general task has revealed fundamental in many application domains, including material science [30], chemistry [41], environmental science [50], forest monitoring [52], and urban analysis [16], to mention a few. In terrain analysis, in particular, the segmentation of a terrain according to its critical points (i.e., peaks and pits) provides information regarding terrain morphology, which are fundamental for assessing the risk of landslides or floods. Terrain surfaces are usually described by either Triangulated Irregular Networks (TINs), or raster-based Digital Elevation Models (DEMs). Although TINs can better adapt to irregularly distributed data, their usage is limited by their large storage costs compared to DEMs. At the same time, the increasing availability of large point clouds [42] intensifies the need for scalable data representations for TINs.

Spurious critical points, naturally affecting noisy data, can severely affect the analysis of a terrain. For this reason, several simplification approaches capable of removing spurious features while maintaining important critical points have been defined in the literature [2, 8, 36, 38]. These approaches reduce the morphological complexity of the dataset, leaving the underlying digital terrain model unchanged. This represents still an issue when working with large terrain datasets since the complexity of extracting, representing, and visualizing topological features and structures is directly related to the resolution of a terrain model. At the same time, reducing the terrain model's resolution may affect its topology in an uncontrolled way.

In [33], we recently addressed this problem by defining a local simplification operator, called *gradient-aware edge contraction*, capable of reducing the resolution of a TIN while preserving the

SIGSPATIAL '21, November 2–5, 2021, Beijing, China

ACM ISBN 978-1-4503-8664-7/21/11…$15.00
https://doi.org/10.1145/3474717.3484261

topology of the underlying terrain. By combining such an operator with a topological simplification operator, the user is enabled to simplify the resolution of both the topology and the geometry of a terrain in a completely controlled way. However, when processing large terrains, multiple issues arise. First, encoding the original TIN is memory-demanding, and, thus, there is the need to use efficient representations to reduce memory requirements. Second, performing a large number of simplifications sequentially is time-consuming [33]. This latter directly affects user interactions during data exploration, thus there is a need to develop a parallel simplification strategy.

In this work, we address both issues by designing and implementing a new simplification approach for triangulated terrains. The algorithm performs topology-aware simplification, by extending gradient-aware edge contraction on a highly efficient data structure, the Terrain trees [18], which has been shown to be the most compact representation for triangulated terrains (see Section 6). Moreover, the distributed nature of Terrain trees is used to define a new parallel simplification algorithm (see Section 7). Our approach reduces the geometric complexity of a large triangulated terrain without affecting its morphology and without incurring into limitations due to processing time or space constraints. In Section 8, we experimentally evaluate both the sequential and the parallel topology-aware simplification on Terrain trees.

2 BACKGROUND

In this section, we review some fundamental elements of discrete Morse theory, which is the basis for 2D scalar field topology, but just restricting to triangle meshes. The interested reader is referred to [11, 22] for a complete view of the theory, and its application in shape analysis and visualization.

Morse theory [37] is a mathematical tool studying the relationships between the topology of a manifold shape M and the critical points of a smooth scalar function f defined over M. Based on Morse theory, we can define segmentations of the shape based on the regions of influence and the connectivity of its critical points. *Discrete Morse Theory (DMT)* [22] is a combinatorial counterpart of Morse theory which nicely extends the results of Morse theory to discrete data, and thus it has been used for analysis of 2D and 3D scalar fields [18, 30, 45, 51].

Given a triangle mesh Σ and an elevation function $f : \Sigma \rightarrow \mathbb{R}$ defined on the vertices of Σ, a *(discrete) vector* is defined as a pair of cells of the complex (σ, τ) such that σ is a face of τ. A *gradient pair* can be viewed as an *arrow* formed by a head (k-simplex) and a tail ($(k-1)$-simplex). Recall that a *k-simplex* is the convex hull of $k+1$ points that are affinely independent in $\mathbb{R}$, and k is called the *dimension* of the simplex. In a triangle mesh, a vertex is a 0-simplex, an edge a 1-simplex, and a triangle a 2-simplex, and we have arrows formed by a triangle and an edge (*triangle-edge pair*), and by an edge and a vertex (*edge-vertex pair*). A simplex that is not a head or a tail of any arrow is a *critical simplex*. In a triangle mesh, there are three types of critical simplices: critical triangles indicating maxima, critical edges indicating saddles, and critical vertices indicating minima. It has been proved that critical simplices appear in correspondence of critical points of the terrain [25].

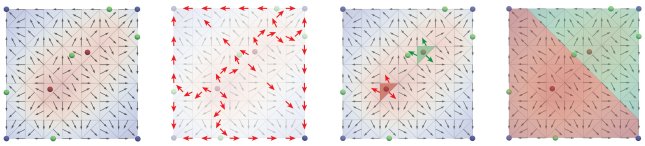

(a) (b) (c) (d)

Figure 1: (a) Forman gradient, (b) V-paths connecting pairs of critical simplices. Regions of influence of critical simplices are computed visiting the V-paths (c) at the critical simplices, and (d) until the whole region of influence is visited.

A *discrete vector field* V is any collection of vectors such that each cell of V is a component of at most one vector in V. A *V-path* is a sequence of vectors (σ_i, τ_i) belonging to V, for $i = 0, \ldots, r$, such that, for all indexes $0 \leq i \leq r-1$, σ_{i+1} is a facet of τ_i and $\sigma_i \neq \sigma_{i+1}$. A V-path is said to be *closed* if $\sigma_0 = \sigma_r$, and *trivial*, if $r = 0$. Discrete vector field V is a *Forman gradient* if all of its closed V-paths are trivial. Figure 1(a) shows an example of a discrete gradient computed on a triangle mesh. Red, green, and blue dots indicate critical triangles, edges, and vertices, respectively. Arrows indicate gradient vectors.

For terrain analysis, the Forman gradient can be seen as the combinatorial counterpart of the gradient of the elevation function f [45, 51] and directly allows the computation of different topological structures [11]. Figure 1(b) shows the gradient paths connecting pairs of critical cells (i.e., critical net). Moreover, the Forman gradient is also used to segment a dataset based on the regions of influence of its critical cells. Figure 1(c) shows the regions of influence for two critical triangles (maxima). Each region of influence is computed by starting from the gradient vectors outgoing the critical triangle and expanding the region recursively until no more gradient vector can be visited (see Figure 1(d)).

3 RELATED WORK

Topology-aware simplification combines the need for reducing the size of a mesh with the need to maintain its topological properties. The task of mesh simplification has been extensively studied in the literature, and, thus, we refer the reader to comprehensive surveys on the topic [6, 31, 49].

Popular techniques for mesh simplifications include edge collapse [32], vertex decimation [48], and vertex clustering [46]. *Edge collapse*, also called edge contraction, consists of the contraction of one edge to a single vertex. When the edge is contracted to one of its endpoints, this operation is called *half-edge collapse*. In this paper, we adopt the half-edge collapse operator as it is the most commonly used one, and does not introduce a new vertex when contracting an edge.

After selecting a simplification operator, one should define the order in which simplifications are performed. When considering edge contraction, several metrics have been defined for optimizing the quality of output meshes, such as minimizing an energy function [32], setting a threshold on the Hausdorff distance between the original and the simplified models [34], minimizing the error quadrics [26], or setting a threshold on the error volume [28]. The

Quadric Error Metric (*QEM*) [26] is one of the few approaches keeping a good balance between the computational cost and the quality of the mesh produced.

Besides the quality of the output mesh, another issue addressed in the literature is to efficiently simplify large meshes. A common and well established method is to perform a simplification on the mesh in parallel or on a cluster. One approach to achieve that is to define heuristics to avoid contracting adjacent edges concurrently [27, 35, 40]. A different strategy is partitioning the mesh into submeshes that can be then processed independently [3, 13, 23, 44].

In this work, we focus on topology-preserving simplifications, i.e., a simplification combining the need to reduce the size of a mesh with the need to maintain its topological properties, such as peaks and valleys. In general, simplification operators are not topology-preserving, which means they can modify the number of critical points of terrain, or their connectivity, in an uncontrolled way.

This problem has been first addressed in [1] by introducing a simplification operator which preserves the critical points of the terrain. The operator removes a vertex from the terrain and re-triangulates the neighborhood such that the remaining vertices maintain the same classification (i.e., minimum, saddle, maximum, non-critical). The method preserves the topology of the terrain, but it lacks an efficient implementation for re-triangulating the terrain.

In [10], the first efficient topology-aware operator based on edge contraction has been introduced. The method preserves the critical points connectivity by checking the separatrix lines incident at the endpoints of a contracted edge. However, while the operator prevents the removal of existing critical points, it does not avoid the creation of new ones.

The first topology-aware simplification based on discrete Morse theory is introduced in [33]. The operator, called *gradient-aware edge contraction*, is able to preserve both the critical simplices and their connectivity by using a Forman gradient as the underlying descriptor of the terrain topology. Before contracting an edge e, the operator checks the gradient pairs in the neighborhood of e. If these pairs are organized in a valid configuration (see Section 5 for details), the contraction is guaranteed to preserve the terrain topology. On top of that, a multiresolution model, called a *Hierarchical Forman Triangulation (HFT)*, is introduced. This model combines geometric and topological operators to enable the mesh simplification or refinement by varying the resolution of both topology and geometry on-demand.

Starting from the gradient-aware simplification operators, the original criteria have been relaxed in [15] to allow the removal of critical simplices. While this operator does not lead to a multiresolution model like HFT, it increases the number of admissible edge contractions, and thus, the compression factor. Recently, a new approach based on vertex removal has been proposed in [24]. The simplification operator is similar to the one introduced in [1], but in this case the topology is preserved by checking a descriptor which definition is rooted in algebraic topology, i.e., persistent homology [17]. A vertex removal is valid only if the link of the removed vertex can be re-triangulated preserving persistent homology.

In this work, we use the gradient-aware edge contraction from [33]. Differently from the vertex removal [24], this operator comes with several metrics for controlling and optimizing the quality of the output meshes [26, 28, 32, 34]. Also, any simplification sequence performed with this operator supports the construction of a HFT multiresolution model which is fundamental if we want to enable a user to explore a dataset interactively in real time.

4 TERRAIN TREES

In this section, we briefly introduce the data structure used in our work. We refer the reader to the original paper for more details [18]. A variety of data structures have been developed for triangle meshes, and the most compact of them encode only the vertices and the triangles of the mesh [12]. Within this class of data structures we can find the Indexed data structure with Adjacencies (IA data structure) [43], the Corner Table (CoT) [47] and the Sorted Opposite Table (SOT) [29]. Recently, a new compact family of spatial data structures designed for triangulated terrain meshes, called *Terrain Trees*, has been developed [18]. Based on Terrain trees, we have developed the *Terrain Tree library (TTL)*, a library for terrain analysis, which contains a kernel for connectivity and spatial queries, as well as modules for morphological terrain analysis and for extracting topological structures, based on the discrete Morse gradient. Terrain trees are based on different nested subdivision strategies of the TIN domain D, which led to three data structures, called PR, PM and PMR Terrain trees, resepectively [18]. In our experiments, the PR Terrain tree has been shown to be slightly more compact and efficient than the other two. So, we will use here the PR Terrain tree, that we will just call Terrain tree, for the sake of simplicity.

A Terrain tree on a triangle mesh Σ consists of: (1) a global vertex array Σ_V, encoding, for each vertex, its coordinates and elevation, (2) a global triangle array Σ_T, encoding, for each triangle, a triplet of vertex indices in the global vertex array, (3) a bucketed quadtree T describing the nested subdivision of D which acts as a bucketing structure for the mesh vertices, and (4) a list of leaf blocks B obtained from the subdivision of D, in which each leaf block b contains the vertices of the mesh that fall in b plus the triangles that intersect b.

Each leaf block contains the minimum amount of information required for extracting all connectivity relations, encoded through a compression method based on sequential range encoding (SRE), introduced in [21]. This method combined with a reindexing of the two global vertex and triangle arrays enables a Terrain tree to encode a triangle mesh with low storage cost, with about 36% less storage than the most compact state-of-the-art mesh data structure (the IA data structure), while maintaining good performances in extracting connectivity relations. Moreover, the hierarchical domain decomposition of Terrain trees makes them well-suited for parallel computation since different leaf blocks can be processed at the same time. These features make Terrain trees more scalable than other triangle-based data structures, and desirable for representing large triangle meshes.

5 TOPOLOGY-AWARE EDGE CONTRACTION

Edge contraction is a widely used operator for triangle mesh simplification [32]. Given an edge $e = \{v_1, v_2\}$ in a triangle mesh Σ, it contracts e to one of its endpoints, and removes from Σ edge e, one of its endpoints, and the triangles incident in e. An edge contraction operator can modify the shape of the TIN creating non-valid meshes. To prevent this, we verify that contracting an edge e

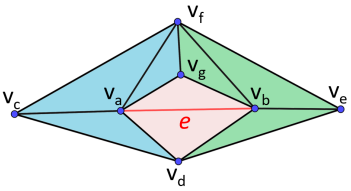

Figure 2: Example of edge contraction not satisfying the link condition. Given edge $e = \{v_a, v_b\}$, we have $Lk(v_a) \bigcap Lk(v_b) = \{v_d, v_g, v_f, \{v_f, v_g\}\}$ and $Lk(e) = \{v_g, v_d\}$. The condition is not verified since $Lk(v_a) \cap Lk(v_b)$ contains vertex v_f and edge $\{v_f, v_g\}$ that are not in $Lk(e)$.

satisfies two fundamental validity conditions, namely the link and the fold conditions.

The *link condition* [14] ensures that the simplified mesh has the same homological properties as the original one. The *link* $Lk(v)$ of a vertex v consists of all vertices adjacent to v in the mesh and of all edges opposite to v bounding the triangles incident in v. Similarly, the link $Lk(e)$ of an edge e consists of the two vertices of the triangles incident in e that are not endpoints of e. An edge $e = \{v_1, v_2\} \in \Sigma$ is said to satisfy the *link condition* if and only if $Lk(v_1) \cap Lk(v_2) \subseteq Lk(e)$. Figure 2 shows an example of an edge contraction that does not satisfy the link condition. If edge e is contracted, the resulting mesh is invalid since more than two triangles would be incident in the same edge (i.e., edge $\{v_f, v_g\}$).

The *fold condition* [5, 26] ensures that, for every edge e' in $Lk(v_2)$, v_1 and v_2 lie on the same side of the line l extended from e'. If this condition is not verified, then Σ will have at least a triangle folding over itself after contracting e to v_1.

Our purpose is to preserve the topological features of the scalar field defined on Σ, while simplifying the underlying mesh. This translates into maintaining the Forman gradient, and thus the critical simplices. To this aim, we apply the *gradient-aware condition* [33]. Given a mesh Σ endowed with a Forman gradient V, an edge $e = \{v_1, v_2\}$ can be contracted to vertex v_1 if and only if: (1) all simplices to be removed (v_2, e, and two triangles incident in e) are not critical; and (2) either v_1 or v_2 is paired with e in V.

A gradient-aware edge contraction requires, in addition to the modification of the mesh, also the update of the Forman gradient V. When contracting edge e, two triangles t_1 and t_2 adjacent to e are removed. The updates of V involve at most four triangles, which share an edge different from e with either t_1 or t_2.

Since the updates are symmetric with respect to e, we only discuss the updates on the left part of e, where edge e is considered as oriented from v_1 to v_2. We denote the other two triangles adjacent to t_1 as t_3 and t_5 and the vertex opposite to e in t_1 as v_3. The updates on the left part need to ensure that vertices v_1, v_3, edge $\{v_1, v_3\}$, and triangles t_3 and t_5 are still paired after simplification. We know that edge e is paired with either v_1 or v_2. Thus, if e is paired with v_2, after the contraction, the pairing of v_1 does not change; otherwise, v_1 will be paired with the simplex paired originally to v_2.

Now consider edges $\{v_1, v_3\}$ and $\{v_2, v_3\}$. Before the contraction, t_1 should have been paired with either $\{v_1, v_3\}$ or $\{v_2, v_3\}$, since edge e was paired and t_1 was not a critical triangle. If t_1 was paired

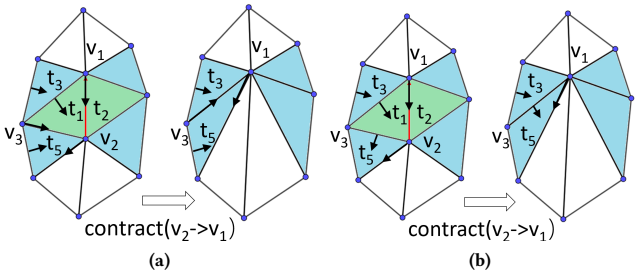

Figure 3: Two possible gradient configurations and corresponding updates after contracting edge $\{v_1, v_2\}$ (in red) to v_1. Black arrows represent gradient pairs.

with $\{v_1, v_3\}$, then $\{v_2, v_3\}$ should have been paired either with one of its endpoints (see Figure 3(a)), or with another triangle, t_5 (see Figure 3(b)). In both cases, t_3 and t_5 are paired with the same simplexes after the contraction. After the removal of t_1 because of the edge contraction, edge $\{v_1, v_3\}$ is paired with the simplex originally paired with edge $\{v_2, v_3\}$, i.e., either with one of its endpoints (see Figure 3(a)), or with another triangle t_5 (see Figure 3(b)). The same reasoning applies when t_1 was paired with $\{v_2, v_3\}$. The same update strategy is applied to the simplices on the right of the edge e to maintain the topology of the discrete gradient [33].

6 TOPOLOGY-AWARE SIMPLIFICATION ON TERRAIN TREES

In this section, we describe a new topology-aware simplification algorithm we developed on a Terrain tree T to simplify a triangle mesh Σ. To preserve the topology of the scalar field (elevation for terrains), the algorithm uses a Forman gradient V computed on Σ inside the Terrain tree and encoded as a bit vector using the same indexing of Σ_T, resulting in a cost of one byte per triangle [51]. As an error metric for edge contraction we use the *Quadric Error Metric* (*QEM*) [26]. For brevity, we describe in Appendix A.1 how to compute the initial error quadrics associated with each vertex v, which represent a set of planes incident in v.

All leaf blocks in Terrain tree T are visited through a depth-first traversal. Algorithm 1 provides a pseudo-code description of the simplification procedure within a leaf block b. The cost of each edge e, which is the error introduced if e is contracted, is computed from the initial error quadrics of its endpoints. In our implementation, edge $e = \{v_1, v_2\}$ is contracted to either v_1 or v_2 depending on which vertex leads to the smallest cost for edge e. We consider e as a *candidate edge* for leaf block b only if the vertex to be removed is contained in b, and the cost of e is lower than a user-defined threshold ω. Edge e is an *internal edge* for b if also the other vertex of e is in b, otherwise e is a *cross edge*.

For each leaf block b, the algorithm performs the following steps:

(1) *Extract the Vertex-Triangle (VT) relations for the vertices in* b (row 1): the *Vertex-Triangle (VT) relation* for a vertex v in b is defined as the set of triangles incident in v.
(2) *Build a priority queue* Q *of candidate edges* (row 3): the edges in the queue are ordered by their cost.

Algorithm 1 LEAF_SIMPLIFICATION(b, Σ, V, E, ω, C, b_R)

Input
b: current leaf block
Σ: the TIN
V: the Forman gradient on Σ
E: the array of vertex error quadrics
ω: the edge cost threshold
C: LRU cache
b_R: root block of the hierarchy

// *Extract the local VT relations for the vertices in* b
1: $local\_vts \leftarrow$ LOCAL_VT(b, Σ_T)
// *Create an array for encoding the updated edges costs*
2: $updated\_edges \leftarrow [\,]$
// *Create a priority queue of candidate edges*
3: $Q \leftarrow$ CANDIDATE_EDGES(b, Σ_T, E, ω)
4: **while** $Q \neq \emptyset$ **do**
5: $e \leftarrow$ DEQUEUE(Q) // e = $\{v_1, v_2\}$
// *Check if* e *has been updated and if its cost is updated*
6: **if** $e \in updated\_edges$ **and not** SAME_COST(e, $updated\_edges$)
7: **then**
8: skip e // *If its cost is not updated, then skip this edge*
9: **end if**
10: $VT(v_1) \leftarrow$ GET_VT(v_1, $local\_vts$, C, b_R, Σ)
11: $VT(v_2) \leftarrow$ GET_VT(v_2, $local\_vts$, C, b_R, Σ)
12: $ET(e) \leftarrow$ GET_ET(e, $VT(v_1)$)
// *Check three conditions introduced in Section 5 for* e
13: **if** LINK_CONDITION(e, $VT(v_1)$, $VT(v_2)$, $ET(e)$)
14: **and** FOLD_CONDITION(e, $VT(v_2)$, $ET(e)$)
15: **and** GRADIENT_CONDITION(e, $VT(v_2)$, $ET(e)$, V)
16: **then**
17: CONTRACT(e, $VT(v_2)$, $ET(e)$, E, Σ)
18: UPDATE_GRADIENT(e, $VT(v_1)$, $VT(v_2)$, $ET(e)$, V)
19: UPDATE_INDEX(e, $VT(v_2)$, b, b_R)
// *Update the VT relation of* v_1
20: VT(v_1) $\leftarrow VT(v_1) \cup VT(v_2)$ - $ET(e)$
// *Update the cost of edges, and add these edges to* Q
21: $updated\_edges \leftarrow$ UPDATE_COSTS(v_1, $VT(v_1)$, E, Q)
22: **end if**
23: **end while**
24: $C \leftarrow C \cup local\_vts$ // *Add local_vts to the LRU-cache*

(3) *Simplify candidate edges* (rows 4-23): for each candidate edge e, the three validity conditions (introduced in Section 5) are checked. If these conditions are satisfied, edge e is contracted, and the Forman gradient updated together with the Terrain tree. This step is described in details below.

The link, fold and gradient-aware conditions are checked for each edge $e = \{v_1, v_2\}$ extracted from Q (row 5). To check these conditions we need the VT relations for v_1 and v_2 and the *Edge-Triangle (ET) relation* of e (rows 10-12). $ET(e)$ consists of the two triangles sharing edge e. If e is an internal edge, $VT(v_1)$ and $VT(v_2)$ in function GET_VT are encoded in array *local_vts*. Conversely, if e is a cross edge, and v_1 is contained by another leaf block b_1, GET_VT must extract the VT relations of b_1. To optimize this latter step, we use an auxiliary Least Recent Used (LRU) cache C for encoding a subset of the extracted VT relations. When v_1 is in block b_1, GET_VT looks first if the VT relations of block b_1 are in C. If such relations are not in C, then we extract them and save them in C.

The ET relation of a candidate edge e is extracted by traversing $VT(v_1)$ and finding triangles incident to e (GET_ET procedure at row 12). To check the link condition (row 13), the set of vertices adjacent to v_1 or v_2 are extracted on-the-fly in LINK_CONDITION by traversing the VT relations of v_1 and v_2.

If e satisfies all three conditions, then it is contracted to its optimized position (i.e., v_1) by function CONTRACT (row 17). This procedure takes as input edge e, the VT relation of v_2, the ET relation of e, the array of vertex error quadrics E, and TIN Σ. It removes vertex v_2 as well as the two triangles adjacent to e. In each remaining triangle in $VT(v_2)$, it replaces v_2 with v_1. After the contraction, the error quadric of v_1 is updated by adding the quadric of v_2 to it. The pseudo-code of function CONTRACT is in Algorithm 2 (see Appendix A.2).

After the contraction, both the Forman gradient V and the Terrain tree T are updated (rows 18-20). The update of gradient V (UPDATE_GRADIENT procedure at row 18) follows the method introduced in Section 5. This involves up to four triangles adjacent to triangles in $ET(e)$ (see Figure 3 for an example). Such triangles are retrieved by using the corresponding VT and ET relations.

The update of T is performed by function UPDATE_INDEX (row 19). If e is an *internal edge*, the current leaf block b is updated by removing the index of v_2 and the indexes of the triangles incident in e. If e is a *cross edge* and v_1 is indexed in leaf block b_1, then both b and b_1 are updated in a similar way. In this latter case, the indexes of those triangles that were incident in v_2 but not encoded in b_1 are also added to b_1. The VT relation of vertex v_1 is updated by adding the triangles in the VT relation of v_2 and by removing the triangles adjacent to e (row 20).

Since the error quadric of v_1 is updated after the contraction of e, the costs of all edges currently incident in v_1 need to be updated accordingly (row 21). A local auxiliary array *updated_edges* which is initialized in row 4, is used to keep track of the updated edge costs. All updated edges are added to Q again. Note that we do not update the costs of edges in Q directly, and, therefore, each time we process an edge e from Q, we check if e has been updated in previous contractions (row 6). If e has been updated and the cost stored with e is not the one stored in *updated_edges* then we discard e and process the next edge in Q.

Finally, after the simplification of leaf block b, the *local_vts* array is inserted to C (row 24).

7 PARALLEL TOPOLOGY-AWARE EDGE CONTRACTION ON TERRAIN TREES

In this section, we propose a parallel algorithm that extends and enhances the algorithm described in Section 6. The hierarchical domain decomposition of Terrain trees makes them well-suited for parallel computation since different leaf blocks can be processed at the same time. Thus, the key idea behind our parallel simplification strategy is to assign each leaf block to a single thread from a set of available threads. The main challenge here is to prevent conflicts that may occur if two threads modify the same vertex, or the same triangle concurrently.

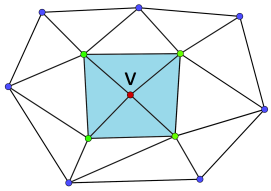

Figure 4: An example of 1-neighborhood (vertices in green) and 2-neighborhood (vertices in green and vertices in blue) of vertex v.

To avoid conflicts between two different threads, we have developed a *leaf locking strategy*, which is based on the definition of *conflict block*. We say that a leaf block b_0 is a *conflict block* for another leaf block b_1, if there exists a cross edge $e = \{v_1, v_2\}$, with v_1 in b_0 and with v_2 in b_1. Clearly, in this case, b_1 is a conflict block for b_0 as well.

There are four possible statuses a leaf block b can have: (1) *default*; (2) *active*; (3) *conflict*; and (4) *finished*. A leaf block b is *active* when it is being processed. A leaf block b is in the *default* status if b is not currently processed and b is not a conflict block of any *active* block. A conflict block of an *active* block is set to the *conflict* status. When the simplification process is completed, block b has status *finished*. A leaf block b can be processed only if its status is *default* and none of its conflict blocks has *conflict* status.

We prove here that this *leaf locking strategy* ensures that no conflict will occur between threads during a parallel simplification process. Given a vertex v in Σ, we define the set of vertices adjacent to v in Σ, as the *1-neighborhood* of v. We then define the *2-neighborhood* of v as the set of vertices that share an edge with any vertex in the 1-neighborhood of v excluding v itself. Note that in such a definition, the 1-neighborhood of v is a subset of its 2-neighborhood. An example of 1-neighborhood and 2-neighborhood of v in Σ is shown in Figure 4.

Let us consider an edge $e = \{v_1, v_2\}$ being contracted to v_1 on Σ. We need to ensure that: (1) the check on e is not affected by other threads, and (2) the update of Σ, the Forman gradient V, and the vertex error quadrics after contracting e, do not conflict with any update operations started by other threads.

From the definitions of 2-neighborhood and of the leaf locking strategy, we have the following:

Proposition 7.1. *Any vertex belonging to the 2-neighborhood of v_2 cannot be removed by any thread while edge $e = \{v_1, v_2\}$ is being processed, and v_2 is the vertex to be removed.*

From Proposition 7.1, we have that no triangle in the VT relations of v_1 or v_2 can be modified by other threads. Therefore the validation of link and fold conditions, and the update of Σ after contracting e cannot be affected by other threads. Similarly, the error quadric of vertex v_1 can only be updated by a single thread, otherwise the other vertex being removed is in the 2-neighborhood of v_2. Although it is possible that the cost of an edge incident in v_1 is updated by a different edge contraction operation, with the other vertex of the edge not being modified, it is easy to prove that such edge is not a candidate edge of current *active* blocks. We refer to Appendix A.3 for the proof.

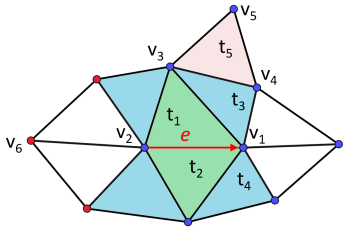

Figure 5: An example of edge contraction on edge $e = \{v_1, v_2\}$ (in red), where v_2, t_1, and t_2 are removed by the contraction. Gradient pairing information of cyan triangles can be modified due to the contraction of e. Red vertices are redirected from v_2 to v_1 after the contraction.

We discuss now how to check and update the Forman gradient V during parallel simplification. From the description of the gradient-aware edge contraction in Section 5, we have that:

Proposition 7.2. *The gradient pairing information associated with triangle t can be modified during the contraction of edge e only if t is adjacent to a triangle incident in e, i.e., adjacent to a triangle to be removed during the contraction of e.*

The validation of the gradient condition involves only the triangles in VT(v_2). It is straightforward to prove that if another edge contraction operation is modifying the gradient pairing information of a triangle in VT(v_2), then the vertex to be removed by that operation is in the 2-neighborhood of v_2 and, thus, breaks the leaf locking strategy condition.

We prove that the gradient pairing information associated with a triangle cannot be modified by two threads at the same time. Suppose triangle t_3 in Figure 5 is modified by two threads Th_1 and Th_2 at the same time and edge e is being removed by Th_1. From Proposition 7.2, we know that t_3 should be adjacent to two triangles being removed by Th_1 and Th_2, respectively. Without loss of generality, we assume that t_5 (purple triangle in Figure 5) is a triangle to be removed by Th_2. Then, either $\{v_4, v_5\}$ or $\{v_3, v_5\}$ is the edge to be removed by Th_2. In both cases, the vertex to be removed is in the 2-neighborhood of v_2, which violates Proposition 7.1.

The parallel simplification strategy performs the following steps:

(1) *Generating auxiliary data structures*: The list of all conflict blocks of a leaf block b, denoted as $Cl(b)$, is computed by traversing all triangles encoded in b. Given a triangle t with at least one vertex in b, we check if the other two vertices of t are also in b. If a vertex v of t is not in b, then, we locate the block b_i containing v, and add b_i to $Cl(b)$.
(2) *Computing the initial error quadrics*: The initial error quadric of each vertex is computed using a parallel version of the algorithm introduced in Appendix A.1.
(3) *Simplification*: each leaf block is simplified by a thread following the steps described in Algorithm 1 with one difference. Each thread needs to update the list of conflict blocks which changes due to the undergoing simplifications, as described below.

Assume a *cross edge* $e = \{v_1, v_2\}$ is contracted to vertex v_1, with v_1 in block b_1 and v_2 in block b_2. Note that e is simplified only when

b_2 is a block with *active* status. Vertices adjacent to v_2, but not to v_1 (for instance, red vertices in Figure 5), are connected to v_1 after contracting edge e to v_1. For example, if vertex v_6 is not encoded in either b_1 or b_2, the edge connecting v_6 and v_1 is a cross edge and may create a new conflict block for b_1.

To update the list of conflict blocks after the contraction of a cross edge, we modify the LINK_CONDITION procedure (row 13 of Algorithm 1) to extract also an auxiliary array vv_{outer}, which encodes the vertices adjacent to v_2 that are not contained in either b_1 or b_2. After the CONTRACT procedure (row 17 of Algorithm 1), we add a step for updating the conflict block list. To update $Cl(b_1)$ after the contraction of e, we find, for each v' in vv_{outer}, the leaf block b' that contains v', and add it to $Cl(b_1)$ if it has not been added yet. Similarly, b_1 is added to $Cl(b')$ when b' is added to $Cl(b_1)$.

The update of $Cl(b_1)$ and $Cl(b')$, when processing b_2, does not affect the concurrent simplification of other blocks. Thanks to the definition of conflict block, both b' and b_1 are conflict blocks of b_2 and, thus, they cannot be active when b_2 is active. Also, being b' and b_1 in a *conflict* state, none of leaf blocks in their conflict lists can have an *active* state.

In contrast to the sequential algorithm, the parallel one does not use a global LRU cache C for storing VT relations, since it could raise resource conflicts when multiple threads access C at the same time. Instead, a local cache at a thread level provides a safe way to encode just the VT relations of blocks in $Cl(b)$ when processing b. Similar to the sequential case, the local cache is accessed and updated only when simplifying a *cross edge*. Once the simplification of b is finished, the local cache is discarded.

We use OpenMP [9] to process multiple leaf blocks in parallel in a Terrain tree. Notice that, while each step makes use of multi-threading internally, the three steps are organized sequentially, i.e., each step of the pipeline is executed only when the previous one is completed. Since the computations performed in steps 1 and 2 are entirely local to a leaf block, they can be processed in a perfectly parallel manner. In step 3, conflicts among threads can prevent the simplification of a leaf block, and thus, the list of the blocks could be traversed multiple times until all blocks are simplified.

8 EXPERIMENTAL RESULTS

In this section, we evaluate the performances of both the sequential and parallel topology-aware terrain mesh simplification algorithms on the Terrain tree. In subsection 8.1, we compare the performance of the sequential topology-aware simplification on the Terrain trees against our implementation of the most compact triangle-based data structure for meshes, the Indexed data structure with Adjacencies (IA data structure) [43]. In subsection 8.2, we compare the sequential and parallel simplification strategies implemented on the Terrain trees. The source code of the simplification algorithm based on Terrain trees is available at [19].

All the experiments are performed on a dual Intel Xeon E5-2630 v4 @2.20Ghz CPU (20 cores in total), and 64GB of RAM. A total of six TINs, generated from raw point clouds using the *CGAL* library [4], are used in our comparisons. The number of vertices per TIN varies from 25 to 113 million (see Table 1). *Molokai* is a dataset consisting of both hydrographic and topographic point cloud data provided by NOAA National Centers for Environmental Information [39].

Table 1: Overview of experimental datasets. For each terrain, we list the number of vertices $|\Sigma_V|$ and trangles $|\Sigma_T|$.

	Molokai	Great Smokey Mountains	Canyon Lake	Yosemite Rim Fire	Dragons Back Ridge	Moscow Mountain
$\|\Sigma_V\|$	25M	34M	49M	78M	91M	113M
$\|\Sigma_T\|$	50M	68M	98M	155M	182M	226M

Great Smokey Mountains, *Canyon Lake*, *Yosemite Rim Fire*, *Dragons Back Ridge*, and *Moscow Mountain*, are topographic LiDAR point clouds from the OpenTopography repository [42].

The generation of the Terrain tree we use in this paper relies on a single parameter which defines the maximum number of vertices allowed in each leaf block of decomposition, i.e. the *block capacity*. To select the block capacity for each dataset in connection with the mesh simplification task, we establish an initial range for capacity values between 1/100000 and 1/30000 of the total number of vertices in the data set, this is in order to have coarser hierarchical subdivisions, usually beneficial for tasks requiring intense navigation of the hierarchy. Within this range, we have selected ten different capacity values for each dataset, and we have compared the performance in sequentially simplifying the meshes encoded by resulting Terrain tree. Our comparisons have shown that the memory footprint and the compression rate, defined as the ratio between the number of vertices in the simplified mesh and in the original one, do not change significantly when using different capacity values (up to 1.7%). Also, simplification times are highly dataset-dependent, and the best performances are achieved with values in the middle of the tested range. Further details of this experimental evaluation can be found in Appendix A.4. In the following, for each dataset, we use the capacity value showing the best trade-off between simplification time and memory requirements.

8.1 Topology-aware mesh simplification on the Terrain tree and IA data structure

The IA data structure encodes a vertex array, containing the coordinates of the vertices of the TIN plus the elevation, and a triangle array encoding for each triangle t the indexes to its three vertices plus the indexes in the triangle array of the three triangles sharing an edge with t. In our implementation [20], we use an enhanced version which also encodes for each vertex v, the index of one triangle incident in v. Such an optimization allows extracting all vertex-based relations in optimal time, i.e, in time linear in the size of the output, and, thus, highly enhances the efficiency of the IA data structure when performing edge contractions.

Both the Terrain tree and the IA data structure use a priority queue for sorting candidate edges as described in Algorithm 1. The Terrain trees use a local priority queue for candidate edges within each leaf block, while the IA data structure uses a global queue for storing all candidate edges of the TIN. The use of different priority queues leads to a different order in which edges are contracted. To estimate the impact on the simplification process, we first compare

the two approaches analyzing the size of the output TIN when varying the quality control parameter. Given a user-defined threshold ω, we simplify all contractible edges with cost lower than ω. Based on the initial error quadrics, we compute the costs for all edges in Σ, and use the quartile values to set three different thresholds.

Table 2 shows the results obtained. Using a global queue leads to TINs that are about 1% smaller than the one obtained by the Terrain tree. On the other hand, the simplification on the Terrain tree is always faster. When using a larger ω, the Terrain tree is at least twice as fast as the IA data structure. Also, when ω increases, the memory requirements on the IA data structure also increase, while on the Terrain tree they remain stable. While using local queues show a slightly lower compression rate with respect to using a global queue, timings and memory requirements are dramatically in favor of the Terrain tree approach. This is even more relevant when edges are simplified in bulk without setting a specific threshold for the edge cost.

Table 3 summarizes the results obtained when simplifying all contractible edges. Results include timings required for computing initial error quadrics and performing the topology-aware simplification, the memory footprint required by the simplification, and the compression rate. On average, Terrain trees simplify 0.5% less edges than the IA data structure, while they use from 45% to 56% less time than the IA data structure. As shown in Table 3, the memory peak on Terrain trees is approximately 41% less than that of the IA data structure. Due to the higher memory requirements, only three of the experiment datasets can be simplified using the IA data structure.

8.2 Parallel topology-aware mesh simplification on the Terrain tree

We evaluate here the performance of the parallel topology-aware mesh simplification algorithm introduced in Section 7 when using from 1 to 64 threads.

Figure 6 shows the speedup achieved by the parallel simplification algorithm when increasing the number of threads. The approach scales well as long as the number of threads is lower than the number of physical cores (20 in our case). The speedup still slightly increases when using more than 20 threads, but it decreases with more than 40.

The efficiency of the parallel algorithm can be computed as $E = T_1/NT_N$, where T_N is the time for the parallel algorithm using N threads, T_1 is the parallel algorithm using a single thread. Figure 7 shows the results. Note that efficiency decreases with the increasing of the number of threads. This is common for parallel algorithms due to possible load imbalance and overheads during the computation. When using 20 threads, the efficiency of the parallel simplification is 67% on all experimental datasets. With more than 20 threads the efficiency decreases faster. Considering these results, we observe that the best trade-off is achieved when the thread number is equal to the number of available cores.

Finally, we compare the parallel and sequential mesh simplification algorithms using the same Terrain tree, and 20 threads (see Table 3). The parallel simplification strategy provides a 12x speedup compared to the sequential strategy, while still reaching

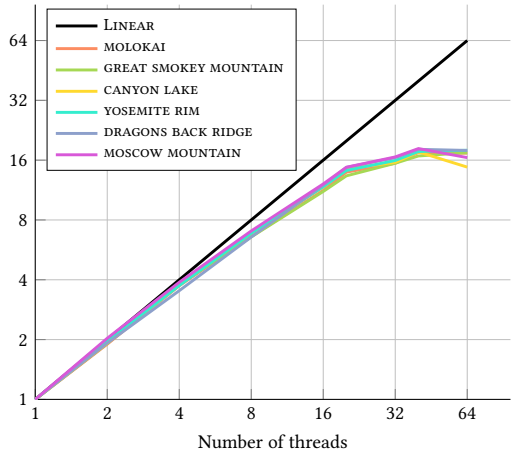

Figure 6: Speedup achieved by the parallel simplification algorithm.

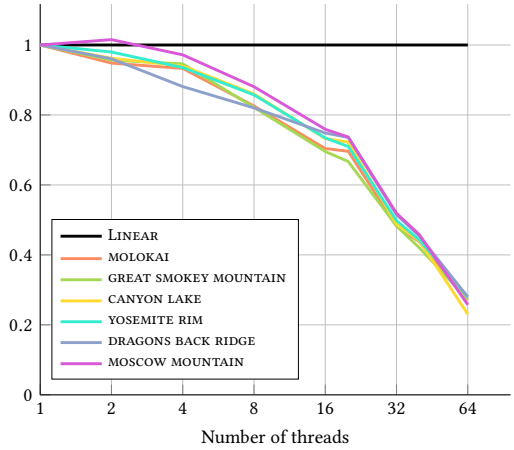

Figure 7: Efficiency achieved by the parallel simplification algorithm.

the same compression rate. Also, even if the parallel strategy processes multiple leaf blocks at the same time, its memory footprint remains stable since, on average, it uses only 1% more memory than that the sequential algorithm. These results show the scalability and efficiency of the Terrain tree representation also when using shared-memory processing techniques.

9 CONCLUDING REMARKS

We have presented a new method for simplifying very large triangle meshes representing terrains on a compact data structure, the Terrain tree. A Terrain tree [18] has been shown to be the most compact data structure for triangulated terrains, which combines a minimal connectivity-based encoding of the triangle mesh with a spatial index as a clustering mechanism that enables an implicit encoding of other connectivity relations.

The simplification method we presented extends the strategy defined in [33] on a global topological data structure, which is

Table 2: Time T (in minutes), peak memory usage M (in Gigabytes), numbers of output vertices $|\Sigma_V|$ and triangles $|\Sigma_T|$ after the simplification on the IA data structure and the Terrain tree (TT) when using different cost threshold ω. Q1, Q2, and Q3 represent the first, the second, and the third quartile edge costs of each dataset, respectively.

	Molokai						Great Smokey Mountain						Canyon Lake					
	IA	**TT**	**IA**	**TT**	**IA**	**TT**	**IA**	**TT**	**IA**	**TT**	**IA**	**TT**	**IA**	**TT**	**IA**	**TT**	**IA**	**TT**
ω	**Q1**		**Q2**		**Q3**		**Q1**		**Q2**		**Q3**		**Q1**		**Q2**		**Q3**	
$\|\Sigma_V\|$	21.5	21.5	17.7	17.7	13.9	13.9	29.1	29.1	24.4	24.4	19.4	19.6	40.9	41	32.8	32.8	26.4	26.4
$\|\Sigma_T\|$	42.9	42.9	35.4	35.5	27.7	27.7	58.2	58.3	48.9	48.9	38.8	39.2	81.8	82.1	65.6	65.7	52.7	52.7
T	13.6	10.5	21.6	13.2	31.8	17.4	15.0	15.0	26.7	20.5	44.3	23	39.4	28.5	79.2	36.1	96.8	39.3
M	17.5	12.7	18.7	12.7	20.0	12.7	23.7	17.2	25.5	17.2	27.2	17.2	34.2	24.6	36.9	24.6	39.2	24.6

Table 3: Time T (in minutes), peak memory usage M (in Gigabytes), and reduction rate R (in %) of topology-aware mesh simplification on the IA data structure, and on sequential (seq.) and parallel (para.) version on Terrain trees.

	Molokai			Great Smokey Mountain			Canyon Lake			Yosemite Rim			Dragons Back Ridge			Moscow Mountain		
	IA	**TT**		**IA**	**TT**		**IA**	**TT**		**IA**	**TT**		**IA**	**TT**		**IA**	**TT**	
		seq.	**para.**		**seq.**	**para.**		**seq.**	**para.**		**seq.**	**para.**		**seq.**	**para.**		**seq.**	**para.**
T	58.0	29.0	2.38	71.0	39.1	3.31	144.1	65.1	5.34	-	100.1	8.12	-	99.8	7.85	-	170.9	13.7
M	21.3	12.7	12.8	29.0	17.2	17.4	41.8	24.6	25.0	O.O.M.	39.0	39.6	O.O.M.	45.9	46.5	O.O.M.	57.4	58.0
R	73.8	73.3	73.4	75.4	75.0	75.0	75.0	74.7	74.7	-	70.6	70.6	-	80.5	80.5	-	77.7	77.7

based on a local simplification operator, called gradient-aware edge contraction, capable of reducing the resolution of a TIN while preserving the topology of the underlying terrain. This operator, paired with a topological simplification operator, reduces the resolution of both the topology and the geometry of a terrain in a completely controlled way. Also, thanks to the distributed nature of Terrain trees, we defined a parallel version of this simplification method. The parallel strategy is based on a leaf locking strategy, that prevents conflicts occurring when multiple threads try to update the same vertex or the same triangle concurrently.

We have experimentally demonstrated how the method based on the Terrain trees can effectively reduce the time and memory requirements of a simplification procedure.

Compared to the IA data structure, which is the most widely used data structure for triangle meshes, and the most compact at the state of the art, Terrain trees require half the time and 40% of the memory while still reaching similar simplification levels. These results prove the scalability and efficiency of our method at processing large-scale triangle meshes. Also, when comparing the sequential and parallel strategies based on Terrain trees, we noticed a further performance increase. Thanks to the local and distributed nature of Terrain trees, the parallel strategy achieves a 12x speedup when using 20 threads while having similar memory requirements.

The parallel strategy developed here can be easily extended to other topology-aware edge contraction operators, such as the one introduced in [15], since the range of simplices involved in those topology-preserving conditions is the same as for our gradient-aware simplification operator. Although the gradient-aware contraction operator is efficient and produces good-quality meshes, some applications requires maintaining the Delaunay property while simplifying the mesh. We plan to investigate how to preserve Delaunay properties in the simplification process, also in connection to coastal ocean modeling for storm surge and tide simulation.

Our current parallel strategy is compatible with a shared-memory processing based on OpenMP [9]. To increase its efficiency, we plan to use specialized compilers, like ISPC[1], and libraries, like TBB[2]. We also plan to extend the simplification algorithm to support a distributed-memory processing strategy based on MPI [7].

ACKNOWLEDGMENTS

This work has been partially supported by the US National Science Foundation under grant number IIS-1910766. It has also been performed under the auspices of the German Aerospace Center (DLR) under Grant DLR-SC-2467209. The Great Smokey Mountains, Canyon Lake, Yosemite Rim Fire, Dragons Back Ridge, and Moscow Mountain point clouds are kindly provided by the OpenTopography Facility with support from the National Science Foundation under NSF Award Numbers 1948997, 1948994 & 1948857. The Molokai point cloud is kindly provided by NOAA National Centers for Environmental Information.

REFERENCES

[1] Chandrajit L. Bajaj and Daniel R. Schikore. 1998. Topology preserving data simplification with error bounds. *Computers & Graphics* 22, 1 (1998), 3–12. https://doi.org/10.1016/S0097-8493(97)00079-4

[2] Peer-Timo Bremer, Valerio Pascucci, and Bernd Hamann. 2009. Maximizing Adaptivity in Hierarchical Topological Models Using Cancellation Trees. In *Mathematical Foundations of Scientific Visualization, Computer Graphics, and Massive Data Exploration.* Springer Berlin Heidelberg, Berlin, Heidelberg, 1–18. https://doi.org/10.1007/b106657_1

[3] Daniela Cabiddu and Marco Attene. 2015. Large mesh simplification for distributed environments. *Computers & Graphics* 51 (2015), 81–89. https://doi.org/10.1016/j.cag.2015.05.015

[1] https://ispc.github.io/

[2] https://software.intel.com/en-us/oneapi/onetbb

[4] CGAL 2021. Computational Geometry Algorithms Library (CGAL). https://www.cgal.org/ [Online; accessed February-2021].

[5] P. Ciarlet and Françoise Lamour. 1996. Does contraction preserve triangular meshes? *Numerical Algorithms* 13 (1996), 201–223.

[6] P. Cignoni, C. Montani, and R. Scopigno. 1998. A comparison of mesh simplification algorithms. *Computers & Graphics* 22, 1 (1998), 37–54. https://doi.org/10.1016/S0097-8493(97)00082-4

[7] Lyndon Clarke, Ian Glendinning, and Rolf Hempel. 1994. The MPI Message Passing Interface Standard. In *Programming Environments for Massively Parallel Distributed Systems*, Karsten M. Decker and René M. Rehmann (Eds.). Birkhäuser Basel, Basel, 213–218.

[8] Lidija Čomić, Leila De Floriani, and Federico Iuricich. 2012. Dimension-Independent Multi-Resolution Morse Complexes. *Computers & Graphics* 36, 5 (Aug. 2012), 541–547. https://doi.org/10.1016/j.cag.2012.03.010

[9] Leonardo Dagum and Ramesh Menon. 1998. OpenMP: an industry standard API for shared-memory programming. *Computational Science & Engineering* 5, 1 (1998), 46–55.

[10] Emanuele Danovaro, Leila De Floriani, Paola Magillo, Mohammed Mostefa Mesmoudi, and Enrico Puppo. 2003. Morphology-Driven Simplification and Multiresolution Modeling of Terrains. In *Proceedings of the 11th ACM International Symposium on Advances in Geographic Information Systems (GIS '03)*. Association for Computing Machinery, New York, NY, USA, 63–70. https://doi.org/10.1145/956676.956685

[11] Leila De Floriani, Ulderico Fugacci, Federico Iuricich, and Paola Magillo. 2015. Morse Complexes for Shape Segmentation and Homological Analysis: Discrete Models and Algorithms. *Computer Graphics Forum* 34, 2 (2015), 761–785. https://doi.org/10.1111/cgf.12596

[12] Leila De Floriani and Annie Hui. 2005. Data structures for simplicial complexes: An analysis and a comparison. In *Proceedings of the third Eurographics symposium on Geometry processing (SGP '05)*. Eurographics Association, Goslar, Germany, 119–128.

[13] Frank Dehne, Chiristian Langis, and Gerhard Roth. 2000. Mesh simplification in parallel. In *Algorithms And Architectures For Parallel Processing (ICA3PP 2000)*. World Scientific, 281–290.

[14] Tamal K. Dey, Herbert Edelsbrunner, Sumanta Guha, and Dmitry V. Nekhayev. 1998. Topology preserving edge contraction. *Publications de l'Institut Mathématique* 66 (1998), 23–45.

[15] Tamal K. Dey and Ryan Slechta. 2018. Edge contraction in persistence-generated discrete Morse vector fields. *Computers & Graphics* 74 (2018), 33–43. https://doi.org/10.1016/j.cag.2018.05.002

[16] Tamal K. Dey, Jiayuan Wang, and Yusu Wang. 2017. Improved Road Network Reconstruction Using Discrete Morse Theory. In *Proceedings of the 25th ACM SIGSPATIAL International Conference on Advances in Geographic Information Systems*. ACM, 1–4. https://doi.org/10.1145/3139958.3140031

[17] Herbert Edelsbrunner and John Harer. 2008. Persistent homology-a survey. *Contemp. Math.* 453 (2008), 257–282.

[18] Riccardo Fellegara, Federico Iuricich, and Leila De Floriani. 2017. Efficient representation and analysis of triangulated terrains. In *Proceedings of the 25th ACM SIGSPATIAL International Conference on Advances in Geographic Information Systems*. ACM, New York, NY, USA, 1–4. https://doi.org/10.1145/3139958.3140050

[19] Riccardo Fellegara and Yunting Song. 2021. Terrain trees library code repository. https://github.com/FellegaraR/Terrain_Trees.

[20] Riccardo Fellegara and Yunting Song. 2021. Terrain_Analysis_on_IA. https://github.com/UMDGeoVis/Terrain_Analysis_on_IA [Online; accessed January-2021].

[21] Riccardo Fellegara, Kenneth Weiss, and Leila De Floriani. 2021. The Stellar decomposition: A compact representation for simplicial complexes and beyond. *Computers & Graphics* (2021). https://doi.org/10.1016/j.cag.2021.05.002

[22] Robin Forman. 1998. Morse theory for cell complexes. *Advances in Mathematics* 134 (1998), 90–145.

[23] Martin Franc and Václav Skala. 2000. Parallel triangular mesh reduction. In *Proceedings of scientific computing (ALGORITMY 2000)*. 357–367.

[24] Ulderico Fugacci, Michael Kerber, and Hugo Manet. 2020. Topology-Preserving Terrain Simplification. In *Proceedings of the 28th International Conference on Advances in Geographic Information Systems (SIGSPATIAL '20)*. ACM, New York, NY, USA, 36–47. https://doi.org/10.1145/3397536.3422237

[25] Ulderico Fugacci, Claudia Landi, and Hanife Varlı. 2020. Critical Sets of PL and Discrete Morse Theory: A Correspondence. *Computers & Graphics* 90 (Aug. 2020), 43–50. https://doi.org/10.1016/j.cag.2020.05.020

[26] Michael Garland. 1999. *Quadric-Based Polygonal Surface Simplification*. Ph.D. Dissertation. Carnegie-Mellon University, Pittsburgh, PA.

[27] Nico Grund, Evgenij Derzapf, and Michael Guthe. 2011. Instant Level-of-Detail. In *Vision, Modeling, and Visualization (2011)*, Peter Eisert, Joachim Hornegger, and Konrad Polthier (Eds.). The Eurographics Association. https://doi.org/10.2312/PE/VMV/VMV11/293-299

[28] André Guéziec. 1999. Locally toleranced surface simplification. *IEEE Transactions on Visualization and Computer Graphics* 5, 2 (1999), 168–189.

[29] T. Gurung and J. Rossignac. 2009. SOT: A compact representation for tetrahedral meshes. In *Proceedings SIAM/ACM Geometric and Physical Modeling (SPM '09)*. ACM, New York, USA, 79–88. https://doi.org/10.1145/1629255.1629266

[30] Attila Gyulassy, Mark Duchaineau, Vijay Natarajan, Valerio Pascucci, Eduardo Bringa, Andrew Higginbotham, and Bernd Hamann. 2007. Topologically Clean Distance Fields. *IEEE Transactions on Visualization and Computer Graphics* 13, 6 (Nov. 2007), 1432–1439. https://doi.org/10.1109/TVCG.2007.70603

[31] Paul S. Heckbert and Michael Garland. 1997. *Survey of polygonal surface simplification algorithms*. Carnegie Mellon University technical report. Carnegie-Mellon Univ Pittsburgh PA School of Computer Science, Pittsburgh, PA.

[32] Hugues Hoppe, Tony DeRose, Tom Duchamp, John McDonald, and Werner Stuetzle. 1993. Mesh Optimization. In *Proceedings of the 20th Annual Conference on Computer Graphics and Interactive Techniques (SIGGRAPH '93)*. ACM, New York, NY, USA, 19–26. https://doi.org/10.1145/166117.166119

[33] Federico Iuricich and Leila De Floriani. 2017. Hierarchical Forman Triangulation: A multiscale model for scalar field analysis. *Computers & Graphics* 66 (2017), 113–123. https://doi.org/10.1016/j.cag.2017.05.015

[34] Reinhard Klein, Gunther Liebich, and Wolfgang Straßer. 1996. Mesh Reduction with Error Control. In *Proceedings of the 7th Conference on Visualization '96 (VIS '96)*. IEEE Computer Society Press, Washington, DC, USA, 311–318.

[35] Hyunho Lee and Min-Ho Kyung. 2016. Parallel mesh simplification using embedded tree collapsing. *The Visual Computer* 32, 6 (2016), 967–976.

[36] Jonas Lukasczyk, Christoph Garth, Ross Maciejewski, and Julien Tierny. 2021. Localized Topological Simplification of Scalar Data. *IEEE Transactions on Visualization and Computer Graphics* 27, 2 (Feb. 2021), 572–582. https://doi.org/10.1109/TVCG.2020.3030353

[37] Yukio Matsumoto. 2002. *An introduction to Morse theory*. Vol. 208. American Mathematical Soc.

[38] John Willard Milnor, Michael Spivak, and Robert Wells. 1969. *Morse theory*. Vol. 1. Princeton University Press, New Jersey.

[39] OCM Partners. 2021. 2013 USACE NCMP Topobathy Lidar: Molokai (HI) . NOAA National Centers for Environmental Information, https://www.fisheries.noaa.gov/inport/item/49753.

[40] Thomas Odaker, Dieter Kranzlmueller, and Jens Volkert. 2016. GPU-Accelerated Real-Time Mesh Simplification Using Parallel Half Edge Collapses. In *Mathematical and Engineering Methods in Computer Science (MEMICS 2015)*. Springer, Cham, Berlin, Heidelberg, 107–118. https://doi.org/10.1007/978-3-319-29817-7_10

[41] Małgorzata Olejniczak, André Severo Pereira Gomes, and Julien Tierny. 2020. A Topological Data Analysis Perspective on Noncovalent Interactions in Relativistic Calculations. *International Journal of Quantum Chemistry* 120, 8 (April 2020). https://doi.org/10.1002/qua.26133

[42] OpenTopography 2020. OpenTopography - High-Resolution Topography Data and Tools. http://www.opentopography.org/ [Online; accessed January-2020].

[43] Alberto Paoluzzi, Fausto Bernardini, Carlo Cattani, and Vincenzo Ferrucci. 1993. Dimension-independent modeling with simplicial complexes. *ACM Transactions on Graphics (TOG)* 12, 1 (1993), 56–102.

[44] Alexandros Papageorgiou and Nikos Platis. 2015. Triangular mesh simplification on the GPU. *Visual Computer* 31, 2 (2015), 235–244. https://doi.org/10.1007/s00371-014-1039-x

[45] Vanessa Robins, Peter John Wood, and Adrian P. Sheppard. 2011. Theory and algorithms for constructing discrete morse complexes from grayscale digital images. *IEEE Transactions on Pattern Analysis and Machine Intelligence* 33, 8 (2011), 1646–1658. https://doi.org/10.1109/TPAMI.2011.95

[46] Jarek Rossignac and Paul Borrel. 1993. Multi-resolution 3D approximations for rendering complex scenes. In *Modeling in Computer Graphics*. Springer, Berlin, Heidelberg, 455–465.

[47] J. Rossignac, A. Safonova, and A. Szymczak. 2001. 3D compression Made Simple: Edge-Breaker on a Corner Table. In *Proceedings Shape Modeling International 2001*. IEEE Computer Society, Genova, Italy.

[48] William J. Schroeder, Jonathan A. Zarge, and William E. Lorensen. 1992. Decimation of Triangle Meshes. In *Proceedings of the 19th Annual Conference on Computer Graphics and Interactive Techniques (SIGGRAPH '92)*. ACM, New York, NY, USA, 65–70. https://doi.org/10.1145/133994.134010

[49] Jo Talton. 2004. *A short survey of mesh simplification algorithms*. Technical report. University of Illinois at Urbana-Champaign. https://truesculpt.googlecode.com/hg/Doc/mesh_simplification.pdf

[50] Akash Anil Valsangkar, Joy Merwin Monteiro, Vidya Narayanan, Ingrid Hotz, and Vijay Natarajan. 2019. An Exploratory Framework for Cyclone Identification and Tracking. *IEEE Transactions on Visualization and Computer Graphics* 25, 3 (March 2019), 1460–1473. https://doi.org/10.1109/TVCG.2018.2810068

[51] K. Weiss, F. Iuricich, R. Fellegara, and L. De Floriani. 2013. A primal/dual representation for discrete Morse complexes on tetrahedral meshes. *Computer Graphics Forum* 32, 3 (2013), 361–370. https://doi.org/10.1111/cgf.12123

[52] Xin Xu, Federico Iuricich, and Leila De Floriani. 2020. A Persistence-Based Approach for Individual Tree Mapping. In *Proceedings of the 28th International Conference on Advances in Geographic Information Systems*. ACM, 191–194. https://doi.org/10.1145/3397536.3422231

A APPENDIX

A.1 Computing the quadric error matrix on Terrain trees

In the Quadric Error Metric (QEM) [26], the error at one vertex v of a triangle mesh Σ is defined as the sum of the squared distances to the planes of the triangles incident in v. The error at v with respect to a plane P is calculated as $\Delta_P(v) = v^T K_P v$, where K_P is a 4×4 matrix called *fundamental error quadric*. The overall error at v can be represented as $\Delta(v) = v^T Q_v v$. Q_v is called *initial error quadric* at v, and is the sum of the fundamental error quadric with respect to the plane defined by each triangle incident in v. The *cost*, or error, introduced by contracting edge $e = \{v_1, v_2\}$ is defined as $\Delta(v) = v^T(Q_1+Q_2)v$, where Q_1 and Q_2 are the initial error quadrics at v_1 and v_2, respectively. The quadric error of v_2 is accumulated to v_1 when e is contracted to v_1. Therefore the cost of e reflects the change from the original mesh to the approximation after the contraction of e.

In each leaf block b, the quadric error matrices E of vertices in b are computed during a traversal of its triangle list. For each triangle t in b:

(1) check if at least one vertex of t contained in b. If not, skip t, otherwise perform step (2);
(2) calculate the fundamental error quadric K_p of the plane on which t lies;
(3) for each vertex v of t, if v is contained in b, add K_p to its initial error quadric $E[v]$.

Note that the fundamental error quadric associated with a triangle may be computed more than once if its vertices are in different leaf blocks. This will slightly increase the computation time compared to traversing through the global triangle array Σ_T of Σ and calculate the corresponding fundamental error quadrics. On the other hand, the computation of the initial error quadrics at the vertices in different leaf blocks are completely independent and fully local to each leaf block. This is optimal for computing the quadric error matrices of Σ in parallel.

A.2 Performing an edge contraction

In this section, we describe how an edge contraction is performed. Algorithm 2 depicts the EDGE CONTRACTION operation at row 17 of Algorithm 1. The algorithm removes the two triangles adjacent to e and vertex v_j (row 2 and row 8). In each remaining triangle in $VT(v_j)$, it replaces v_j with v_i (row 4 to 6). After the contraction, the error quadric of the remaining vertex v_i is updated by adding the quadric of v_j to it (row 7).

A.3 Correctness proof of the parallel simplification algorithm

In this section, we provide the correctness proof of Proposition 7.1 and an explanation of why the possible edge cost conflicts cannot affect the parallel simplification.

We recall Proposition 7.1:

PROPOSITION 7.1. *Any vertex belonging to the 2-neighborhood of v_2 cannot be removed by any thread while edge $e = \{v_1, v_2\}$ is being processed, and v_2 is the vertex to be removed.*

Algorithm 2 CONTRACT(e, VT(v_j), ET(e), E, Σ)

Input
$e = \{v_i, v_j\}$: edge to be contracted to v_i
$VT(v_j)$: the Vertex-Triangle relation of v_j
$ET(e)$: the Edge-Triangle relation of e
E: the array of vertex error quadrics
Σ: the triangulated terrain

1: **for each** t in $ET(e)$ **do**
2: $\Sigma \leftarrow \Sigma - \{t\}$ // *Remove t from Σ*
3: **end for**
// *For each triangle t incident in v_j but not adjacent to e*
4: **for each** t in $(VT(v_j) - ET(e))$ **do**
5: $t \leftarrow (t - v_j) \cup v_i$ // *Replace v_j with v_i in t*
6: **end for**
7: $E[i] \leftarrow E[i] + E[j]$ // *Update the error quadric at vertex v_i*
8: $\Sigma \leftarrow \Sigma - \{v_j\}$ // *Remove v_j from Σ*

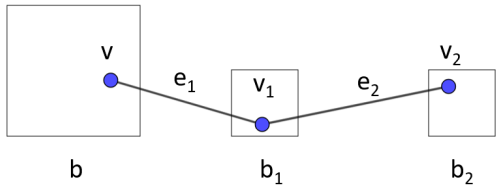

Figure 8: An example of a vertex v and two vertices in its 2-neighborhood.

Consider a vertex v in leaf block b_1 to be removed in an edge contraction operation in the parallel simplification, from the definition of 2-neighborhood, we know that a vertex v' in the 2-neighborhood either is adjacent to v (e.g., v_1 in Figure 8) or has a sharing adjacent vertex with v (e.g., v_2 in Figure 8). We first consider the case that a vertex v_2 shares an adjacent vertex v_1 with v. There are two edges $e_1 = \{v, v_1\}$ and $e_2 = \{v_1, v_2\}$ between v and v_2. There are three possible cases for e_1 and e_2: (1) both of them are internal edges, (2) one of them is an internal edge, the other one is a cross edge, (3) both of them are cross edges. In case (1), v and v_2 belong to the same block and cannot be removed at the same time. In case (2), v_2 belongs to a conflict block of b, while in case (3), v_2 belongs to a block b_2 which shares a conflict block b_1 with b as shown in Figure 8. In both cases, the block encoding v_2 cannot be processed when b is in status *active* according to the definition of leaf locking strategy. Recall that for a leaf block b, an edge is only considered as candidate if the vertex to be removed is encoded in b. Therefore v_2 cannot be removed when the block encoding it is not *active*.

Similarly, when v' is adjacent to v, v' is either in b or in a conflict block of b. In both cases, v' cannot be considered in an edge contraction operation.

In section 7, we proved that the leaf locking strategy ensures that the validation of three conditions and most of the update within an *active* block will not be affected by other threads. But it is possible that the cost of one edge is updated by different threads at the same time. Let us consider an edge $e_1 = \{v_1, v_2\}$ being contracted to v_2

Table 4: Time (in minutes) (denoted as T), peak memory usage (in Gigabytes) (denoted as M), and reduction rate (in %) (denoted as R) of simplification when using different capacity values (denoted as C) for the subdivision of Terrain tree.

Molokai				Great Smokey Mountains				Canyon Lake				Yosemite Rim Fire				Dragons Back Ridge				Moscow Mountain			
C	**T**	**M**	**R**	**C**	**T**	**M**	**R**	**C**	**T**	**M**	**R**	**C**	**T**	**M**	**R**	**C**	**T**	**M**	**R**	**C**	**T**	**M**	**R**
300	36.3	12.8	73.1	300	44.8	17.4	74.7	450	70.9	24.9	74.6	600	104.2	39.5	70.6	600	117.3	46.3	80.4	900	186.4	57.2	77.5
400	35.1	12.8	73.2	400	45.2	17.3	74.9	600	68.7	24.7	74.6	800	99.1	39.4	70.6	900	100.5	46.2	80.4	1200	185.7	57.6	77.5
500	29.5	12.7	73.3	500	39.4	17.3	74.9	750	68.8	24.9	74.6	**1000**	100.1	39.0	70.6	**1200**	99.8	45.9	80.5	1500	192.9	57.1	77.6
600	29.0	12.8	73.3	600	41.9	17.3	75.0	**900**	65.1	24.6	74.7	1200	100.5	39.4	70.6	1500	129.2	46.0	80.6	1800	188.7	57.4	77.6
700	29.0	12.7	73.3	700	39.8	17.3	75.0	1050	68.4	24.9	74.7	1400	100.3	39.4	70.6	1800	126.7	45.9	80.6	2100	172.0	57.5	77.6
800	29.5	12.7	73.4	**800**	39.1	17.2	75.0	1200	66.5	24.6	74.7	1600	100.9	39.3	70.6	2100	127.9	46.1	80.6	**2400**	170.9	57.4	77.7
900	29.1	12.7	73.4	900	39.4	17.3	75.0	1350	66.7	24.8	74.7	1800	102.2	39.2	70.6	2400	131.7	45.7	80.6	2700	176.9	57.3	77.7
1000	29.2	12.7	73.4	1000	39.4	17.3	75.0	1500	73.2	24.8	74.8	2000	106.7	38.9	70.7	2700	131.8	46.1	80.6	3000	176.3	56.9	77.7
1100	29.2	12.8	73.4	1100	39.6	17.4	75.0	1650	75.5	24.7	74.8	2200	111.4	39.3	70.7	3000	129.8	46.1	80.6	3300	177.2	57.3	77.7
1200	29.8	12.7	73.4	1200	39.5	17.3	75.1	1800	73.3	24.6	74.8	2400	106.8	39.2	70.7	3300	129.6	46.0	80.6	3600	173.9	57.2	77.7

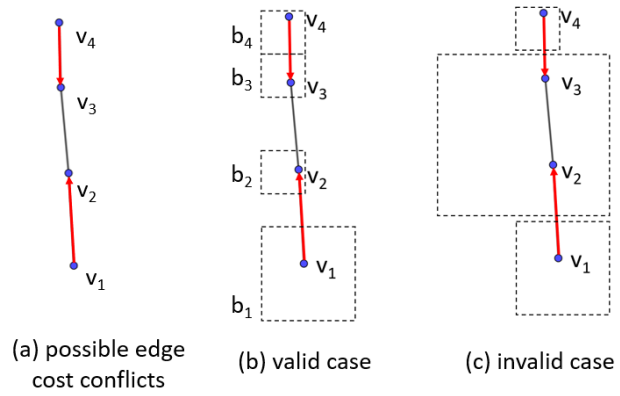

Figure 9: (a) shows an example of a possible conflict occurring when two edges are contracted at the same time (triangles are not displayed for clarity). Edge $e_1 = \{v_1, v_2\}$ is contracted to v_2 and edge $e_2 = \{v_3, v_4\}$ is contracted to v_3. (b) shows a case that blocks encoding v_1 and v_4 can be active at the same time under the leaf locking strategy, and (c) shows an invalid case in which v_1 and v_4 cannot be removed at the same time.

and another edge $e_2 = \{v_3, v_4\}$ being contracted to v_3 on Σ. If v_2 and v_3 are connected by an edge e_0, it is still possible that e_1 and e_2 are contracted by different threads at the same time since v_1 and v_4 are not in each other's 2-neighborhood. Assume that e_1 is contracted on Th_1 and e_2 is contracted on Th_2. If Th_1 updates the error quadric of v_2 and the cost of e_0 before error quadric of v_3 is updated on Th_2, then Th_2 will have a different updated cost of e_0 since it calculates with two updated error quadrics. But such a conflict will not affect the simplification on either thread, since, this case can only happen when e_0, e_1, and e_2 are all cross edges (see Figure 9(b)). Otherwise, like the example in Figure 9(c), leaf blocks encoding v_1 and v_4 must be conflict block of each other and so that e_1 and e_2 cannot be simplified at the same time. When all three edges are cross edges, neither endpoints of e_0 is encoded in the same block as v_1 or v_4, and thus, it is not a candidate edge in these blocks. Therefore although it is possible that the cost of an edge is updated by different threads, such edge is not a candidate edge of current *active* blocks and will not affect the simplification of those blocks.

A.4 Experiments on leaf capacity selection

In this section we present the results in which we evaluate the performance of simplification algorithm when using different capacity thresholds on Terrain trees. Recall that a capacity defines the maximum number of vertices that each leaf block can contain.

Table 4 shows the performances of sequential topology-aware mesh simplification on the Terrain tree. The memory footprint does not change significantly when using different leaf capacities. The same holds for the percentage of edges contracted. Depending on the dataset, timings may vary. For example, on the Molokai dataset, the simplification is 21% faster when a shallower hierarchy (larger capacity) is used, while on Dragons Back Ridge, using a deeper hierarchy (smaller capacity) reduces the simplification time by 24%. The simplification time is stable when the capacity value varies in a small range. Overall, the results show that even selecting a suboptimal capacity for generating a Terrain Tree, performances are not severely affected and the algorithm still performs well. In the paper, we keep only one capacity value for each dataset to use in the experiments. In general, we use the capacity value that leads to the shortest simplification time, but when the variation in time is small (less than 1%), we consider also the memory cost and the reduction rate. The capacity value selected for each dataset is denoted in Table 4 in bold face.